ELSEVIER

Biophysical Chemistry 105 (2003) 449–459

Biophysical Chemistry

www.elsevier.com/locate/bpc

A simple analytical model of water

Thomas M. Truskett[a,*], Ken A. Dill[b]

[a]*Department of Chemical Engineering and Institute for Theoretical Chemistry, The University of Texas at Austin, Austin, TX 78712, USA*

[b]*Department of Pharmaceutical Chemistry, University of California, San Francisco, San Francisco, CA 94143-1204, USA*

Received 16 October 2002; accepted 16 December 2002

Abstract

Water is an unusual liquid. It expands upon freezing, has minima in its volume, heat capacity, and isothermal compressibility with temperature, and shows signs of a first-order phase transition when supercooled. These anomalies disappear at high pressures. We review a recent analytical theory that predicts water's thermal properties and the main features of its phase diagram, including multiple crystalline phases and a fluid–fluid transition in the supercooled liquid. It also predicts a fragile-to-strong crossover in supercooled water's temperature-dependent relaxation processes. The theory is based on a simplified model for how triplets of waters interact via hydrogen bonds, steric repulsions, and dispersion attractions. It is designed to give simple insights into the microscopic origins of water's properties.

Keywords: Water; Statistical mechanics; Analytical model; Hydrogen-bonding; Phase diagram; Thermodynamic anomalies

1. Introduction

Many properties of liquids and solids have been explored through computer simulations of atomically-detailed models. However, some properties of detailed models are difficult to study because of the computational expense. In particular, entropies, heat capacities, and phase diagrams require extensive sampling of phase space. Moreover, some physical properties of materials are nearly universal (e.g. critical phenomena), and thus they are insensitive to the details of intermolecular potential. Hence, we believe there is also a need for simple analytical theories. Analytical models have the potential to treat a broad range of conditions, reveal trends and universal behavior, suggest functional relations for engineering applications, and motivate experiments. Here, we examine the predictions of an analytical model that we recently introduced [1,2] to study water in its liquid and solid phases.

There are some significant challenges in modeling water. For example, temperature and pressure affect 'hot' liquid water (near its boiling point) differently than 'cold' water (near its freezing point) [3–6]. Heating hot water increases its compressibility and heat capacity and reduces its density and refractive index. Heating cold water has the opposite effect. Applied pressure reduces the mobility of the molecules in hot water, but it increases the mobility of cold water. Compression

*Corresponding author. Tel.: +1-512-471-6308; fax: +1-512-471-7060.

E-mail address: truskett@che.utexas.edu (T.M. Truskett).

0301-4622/03/$ - see front matter © 2003 Elsevier Science B.V. All rights reserved.
doi:10.1016/S0301-4622(03)00107-8

melts ice at low pressures, but it freezes the liquid at high pressures.

In addition, supercooled water has interesting properties. Cooling liquid water below its freezing point without crystallization (supercooling) leads to pronounced increases in its isothermal compressibility, isobaric heat capacity, and in the magnitude of its negative thermal expansion coefficient [5]. These behaviors suggest the presence of a thermodynamic singularity in the deeply supercooled fluid. One intriguing possibility is a first-order phase transition between two metastable liquid phases of water [7,8].

Liquid water also has interesting properties as a solvent. Water participates in hydrophobic interactions with non-polar solutes. These interactions, although still poorly understood, are known to be important for self-assembly and aggregation events in aqueous solution including protein folding, the formation of cell membranes, and the binding of drugs to proteins [9–12]. Statistical mechanical theories [13–15] have demonstrated that key aspects of hydrophobic interactions are related to the thermodynamics of water itself. This suggests that a good starting point for studying water's role in solvation–desolvation processes is an accurate molecular theory for pure water.

There is a key limitation in many existing statistical mechanical theories of water. They are not based on a microscopic model of the underlying interactions, such as van der Waals forces and hydrogen bonding; i.e. they do not derive the structural properties of water from energetics. Rather, they begin from experimental observables of equilibrium properties, such as its equation of state or the temperature-dependent water–water pair correlation function. While such models have been quite valuable, they do not address the key question about how the structure of water arises from its energetic interactions.

Perturbation theories have recently been developed to account for the effect of hydrogen-bonding interactions on water's properties [16–19]. These approaches are able to successfully predict a broad range of the experimentally observed properties of stable and supercooled liquid water. However, an important limitation of these models is that they are not able to account for water's solid 'ice' phases, and they are not designed to predict the hydrogen-bonding structures present in the liquid phase.

Here, we review a simple analytical theory [1,2] that is based on a microscopic model for how triplets of water molecules interact via hydrogen bonds, steric repulsions, and van der Waals attractions. The aim is to provide simple insights into the microscopic origins of water's physical properties. We have used it to study the thermal and structural properties of water in its liquid and solid phases. The theory describes water's thermodynamic anomalies, the main features of its equilibrium phase diagram, and the populations of its local hydrogen-bonding structures.

We are happy to dedicate this paper to Walter Kauzmann, whose deep insights into the behaviors of proteins, glasses, and water have motivated much of our work, including the model that is described in the present review.

2. The model

In our model, each water molecule is a two-dimensional disk with three identical bonding arms, separated by 120°, as in the Mercedes Benz (MB) logo. Good hydrogen bonds form when two bonding arms of neighboring molecules are collinear and their molecular centers are separated by a distance *d*. This structure promotes the formation of open hydrogen-bond networks of orientationally-constrained molecules, a key component of water's anomalous behavior [8,17]. The present model bears structural resemblance to the MB model [20], although the energetics of the two models are somewhat different. The MB model has been studied extensively by Monte Carlo simulations [21–23] and is known to reproduce qualitatively the properties of liquid water and hydrophobic effects. Because the MB model can predict the distinctive properties of water, and because it gives insights into the microscopic origins of those properties, we felt it would be valuable to develop an analytical version of this type of model.

2.1. Liquid and vapor phases

The liquid and vapor phases in our model consist of N molecules of diameter d contained

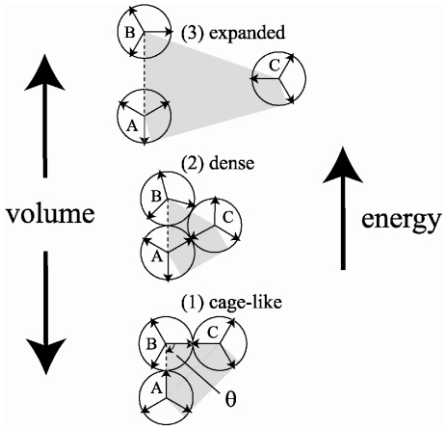

Fig. 1. Cell types for the triplets of waters in the fluid states, shown from bottom to top in order of increasing energy. Cell volumes v_j ($j=1,2,3$) are denoted by the gray shaded house-shaped regions. The triangle that forms the top of the house is defined by the lines that connect the three molecular centers of A, B and C. The base of the house is the rectangle that lies between the line connecting molecular centers of A and C and the parallel line tangent to those molecules. The molecular sectors in one cell sum exactly to the volume of one molecule $\pi d^2/4$. θ is the local orientation of the 'central' molecule B.

within N neighborhoods that we call 'cells'. The cells are indistinguishable and fluctuate between states with different structures, volumes, and energies. These states are (1) *cage-like*, (2) *dense*, and (3) *expanded.* They describe the mutual interaction of a central molecule (labeled B in Fig. 1) and two of its neighbors (A and C). The cage-like and dense cell types correspond roughly to the transient structured and unstructured regions observed in computer simulations [24,25] and experiments [26] of liquid water, while the expanded cell type accounts for the local density fluctuations that give rise to the vapor phase.

One aim of the theory is to predict how temperature T and pressure P affect the populations $f_j(T, P)$ ($j=1,2,3$) of cell types 1 (cage-like), 2 (dense), and 3 (expanded). The sum of these populations obeys the normalization condition

$$\sum_{j=1}^{3} f_j = 1 \tag{1}$$

Fig. 1 shows the *house-shaped* structure that characterizes the local 'volume' that is associated with each cell (we use the term volume instead of area here, to maintain the analogy with three-dimensional water. The quantity we calculate is the area of the house). The sectors of A, B and C that are contained within one house (shaded region, Fig. 1) sum exactly to the volume of one molecule $\pi d^2/4$. The volumes of the N cells sum to the total system volume N_v.

2.1.1. Cage-like cells, type 1

Cell type 1 (Fig. 1) is a low-energy, cage-like triplet structure in which molecule B can rotate subject to two constraints. First, B is constrained to maintain a perfect hydrogen bond with C (i.e. B and C are in contact and their bonding arms are collinear). Second, molecule A contacts B with its bonding arm pointed towards B's center. The potential energy of this cell u_1 has a square-law dependence on the angle θ that describes the local orientation of molecule B:

$$u_1 = \begin{cases} -\varepsilon_{HB} + k_s(\theta - 2\pi/3)^2 & \pi/3 < \theta < \pi \\ -\varepsilon_{HB} + k_s(\theta - 4\pi/3)^2 & \pi < \theta < 5\pi/3 \\ \infty & \text{otherwise} \end{cases} \tag{2}$$

where k_s represents the 'spring constant' associated with bending the A–B bond, and $-\varepsilon_{HB}$ is the energy of the cell's ground-state configuration in which two perfect hydrogen bonds are formed. B cannot access orientations $0<\theta<\pi/3$ or $5\pi/3<\theta<2\pi$ because of the steric repulsions between C and A. The cell volume v_1 of the cage-like structure is

$$v_1(\theta) = a_1(\theta) d^2 \tag{3}$$

where $a_1(\theta) = \sin(\theta/2) \times \left[1 + \left|\cos(\theta/2)\right|\right]$. Eq. (3) is the sum of two contributions to the house: $d^2\sin(\theta/2)$ is the volume of the rectangular base and $d^2\sin(\theta/2) \times \left|\cos(\theta/2)\right|$ is the volume of the triangular roof. Although this volume depends on

θ, we assume that the hydrogen bond is sufficiently stiff (i.e. k_s is sufficiently large) that the cell volume can be approximated [2] as the ground-state value,

$$v_1 \approx \frac{3\sqrt{3}d^2}{4} \tag{4}$$

2.1.2. Dense cells, type 2

Cell type 2 (Fig. 1) is compact: molecules A, B and C are compressed into mutual contact. This structure has van der Waals contacts, but molecule B does not participate in hydrogen bonds with A or C. The cell interaction energy u_2 and volume v_2 are assumed to be constant, independent of B's orientation:

$$u_2 = -\varepsilon_d \tag{5}$$

and

$$v_2 = a_2 d^2 \tag{6}$$

where $a_2 = (2+\sqrt{3})/4$. Here, $d^2/2$ is the volume of the rectangular base and $\sqrt{3}d^2/4$ is the volume of the triangular roof.

2.1.3. Expanded cells, type 3

In this cell type (low local density) (Fig. 1), molecule B does not interact with neighbors A and C (aside from the hard-core overlap constraints),

$$u_3 = 0 \tag{7}$$

we approximate the distribution of volumes of the expanded cell by the average volume of a 1-D excluded volume gas v_3,

$$v_3 = \frac{k_B T}{P} + b \tag{8}$$

where k_B is Boltzmann's constant and we choose $b[sv829?(2+\sqrt{3})d^2/4$ to be the minimal cell size in the fluid.

2.1.4. Cell–cell attractions

To account for interactions beyond the triplet level, we include a global attractive energy $-Na/v$, where a is the van der Waals dispersion parameter and v is the average molar volume.

2.1.5. Statistical mechanics

We develop the equilibrium statistical mechanics of this model within the isothermal-isobaric ensemble (constant N, P and T). We treat the cells in the fluid states as N indistinguishable, weakly interacting (i.e. independent) subsystems, so we express the partition function of the fluid $\Delta(N,P,T)$ as

$$\Delta = \frac{1}{N!}[\Delta_{\text{cell}}]^N \tag{9}$$

Δ_{cell} is the partition function for molecule B in its cell, given by

$$\Delta_{\text{cell}} = c(T)N\sum_{k=1}^{3}\iint_{\{k\}} \mathrm{d}x\mathrm{d}y \int_0^{2\pi} \mathrm{d}\theta \exp\left(-[u_k + Pv_k]/k_B T\right) \tag{10}$$

where $c(T)$ is the normal 2-D momentum contribution [2]. The sum is taken over the three cell types (cage-like, dense and expanded), and (x,y) are the Cartesian coordinates of molecule B (i.e. the central molecule). The double integral $\iint_{\{k\}} \mathrm{d}x\mathrm{d}y$ represents the translational volume that is accessible to molecule B in cell type k.

An approximate analytical expression has been derived [2] for the cell partition function Δ_{cell} in Eq. (10), which leads to the following form for Δ,

$$\Delta = \left(\sum_{j=1}^{3} g_j \exp\left[-\left\{\langle u_j\rangle + Pv_j\right\}/k_B T\right]\right)^N = \left(\sum_{j=1}^{3}\Delta_j\right)^N \tag{11}$$

here $\langle u_j\rangle$ are average energies for the three energy levels $j = 1,2,3$,

$$\langle u_1\rangle = -\varepsilon_{HB} + \frac{k_B T}{2} - \sqrt{k_s \pi k_B T}\,\frac{\exp\left(-k_s\pi^2/9k_B T\right)}{3\mathrm{erf}\left(\sqrt{k_s\pi^2/9k_B T}\right)}$$

$$\langle u_2\rangle = -\varepsilon_d$$

$$\langle u_3\rangle = 0 \qquad (12)$$

and g_j are the corresponding densities of states,

$$g_1(T) = 2\pi d^2 c(T) e \frac{\mathrm{erf}\left(\sqrt{k_s\pi^2/9k_BT}\right)}{\sqrt{k_s\pi/k_BT}}$$

$$\times \exp\left(\frac{1}{2} - \frac{\sqrt{k_s\pi/k_BT}\exp\left[-k_s\pi^2/9k_BT\right]}{3\mathrm{erf}\left(\sqrt{k_s\pi^2/9k_BT}\right)}\right)$$

$$g_2(T) = 2\pi d^2 c(T) e$$

$$g_3(T,P) = 2\pi c(T) e(v_3 - b) = 2\pi c(T) e \frac{k_BT}{P} \qquad (13)$$

the fractional populations of the cell types $f_j(T,P)$ are obtained from Eqs. (11)–(13),

$$f_j = \frac{g_j \exp\left[-\left(\langle u_j\rangle + Pv_j\right)/k_BT\right]}{\sum_{k=1}^{3} g_k \exp\left[-\left(\langle u_j\rangle + Pv_j\right)/k_BT\right]} = \frac{\Delta_j}{\sum_k \Delta_k} \qquad (14)$$

these populations are the fundamental microscopic quantities in the model.

Properties of the liquid and vapor phases can be computed from Δ using standard thermodynamic relations. For example, the chemical potential is given by $\mu(T,P) = -\left(k_BT/N\right)\ln\Delta$, and the molar volume (i.e. the equation of state) is given by $v(T,P) = \left(\partial\mu/\partial P\right)_T$. Truskett and Dill [2] discusses how to account for the global dispersion energy $-Na/v$ when computing the model's thermodynamic properties. In contrast to molecular simulations using atomically-detailed models, thermodynamic properties of the present theory can be computed in a few seconds on a personal computer.

2.2. Crystalline phases

In order to compute the model's phase diagram, we must determine the possible crystalline phases.

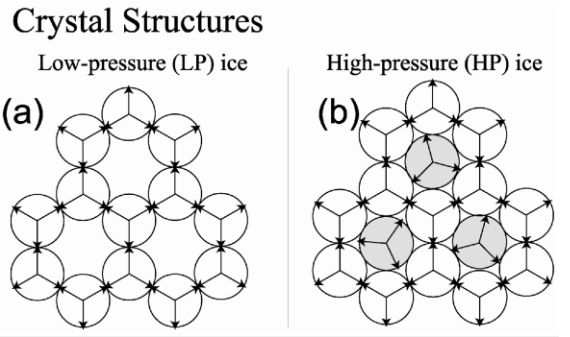

Fig. 2. (a) The structure of low-pressure (LP) ice. (b) The structure of high-pressure (HP) ice. HP ice is identical to LP ice, except that each cage in HP ice has an additional molecule (shaded gray) in its center that does not participate in hydrogen bonds.

As a first step, we consider two types of solids: a low-pressure (LP) ice and a high-pressure (HP) ice. Our choice for the LP phase is simplified by the fact that there is only one possible crystalline arrangement that permits the maximum number of perfect hydrogen bonds per molecule. This low-density crystal structure, shown in Fig. 2a, is analogous to hexagonal ice I_h, and it is also the crystalline phase that has been observed in low-temperature Monte Carlo simulations of the MB model [21].

Water also has denser forms of ice at high pressures. To explore the possible structures of a dense crystalline phase, we recall that there is a unique minimum-volume ($v = \sqrt{3}d^2/2$) arrangement for 2-D disks in the plane. Fig. 2b illustrates one candidate structure, which we call the HP (high-pressure) crystal, which conforms to this triangular packing arrangement.

The two ices described above are not the only possible crystalline structures for this model. However, a preliminary search using our theory has not revealed other stable crystals. Hence, we take the model's LP (low-pressure) and the HP phases as being representative of water's crystalline forms.

We treat the model ices via a cell theory approach in which each solid is composed of N independent cells. We assume that the solids are incompressible and obtain analytical expressions [2] for the chemical potentials of the two ice forms

Table 1
Reduced thermodynamic variables; the subscript C indicates that the quantity is evaluated at the liquid–vapor critical point

Reduced temperature	$T_r = T/T_C$
Reduced pressure	$P_r = P/P_C$
Reduced volume	$v_r = V/V_C$
Dimensionless isothermal compressibility	$\kappa_T^* \equiv -\left(\partial \ln v_r/\partial P_r\right)_{T_r} = \kappa_T P_C$
Dimensionless thermal expansion coefficient	$\alpha_P^* \equiv \left(\partial \ln v_r/\partial T_r\right)_{P_r} = \alpha_P T_C$

Table 2
Parameters for the model

$a/(d^2\varepsilon_{HB})$	0.295
$\varepsilon_d/\varepsilon_{HB}$	0.15
k_s/ε_{HB}	100 000

$\mu_{LP}(T,P)$ and $\mu_{HP}(T,P)$, respectively. Their molar volumes are $v_{LP} = 3\sqrt{3}d^2/4$ and $v_{HP} = \sqrt{3}d^2/2$. A more detailed discussion of the intermolecular interactions and the thermodynamics of the crystalline phases is given in Truskett and Dill [2].

3. Predictions

3.1. Thermodynamic anomalies

Here, we summarize the thermodynamic properties of the model. In order to compare with experiments, we use the reduced variables shown in Table 1. In reduced units, the predictions of the theory depend on three parameters: $a/(d^2\varepsilon_{HB})$, $\varepsilon_d/\varepsilon_{HB}$, and k_s/ε_{HB}. These dimensionless combinations quantify the ratios of the characteristic dispersion energy $-a/d^2$, the dense state energy $-\varepsilon_d$, and the bonding spring constant k_s to the

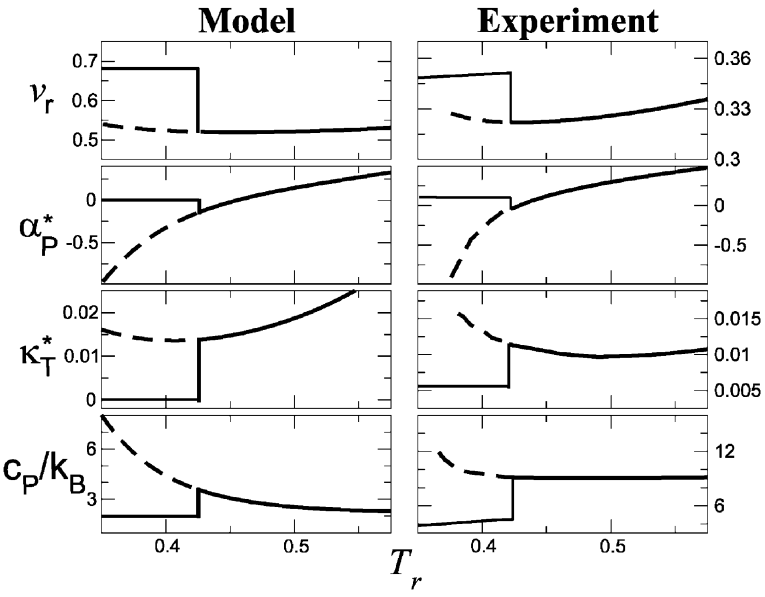

Fig. 3. Water's properties vs temperature T_r at atmospheric pressure (see footnote 1): model predictions (left) and experiment [27–30] (right). Solid lines are the properties of the stable liquid and crystalline phases, and dashed lines are the properties of the supercooled liquid. Discontinuities occur at the first-order freezing transition (see Fig. 6). (a) volume v_r, (b) thermal expansion coefficient α_P^*, (c) isothermal compressibility κ_T^*, and (d) isobaric heat capacity c_p/k_B.

characteristic hydrogen-bonding energy $-\varepsilon_{HB}$. The parameters used to calculate the properties of water are shown in Table 2. Although this parameter set has not been optimized to match any particular property of water, it was found to yield a good overall description of the experimental data.

Fig. 3 compares the predictions for the volume v_r, thermal expansion coefficient α_P^*, isothermal compressibility κ_T^*, and isobaric heat capacity c_P with experimental data [27–30] for water at atmospheric pressure.[1] The model captures liquid water's negative α_P^* and steep increases in v_r, κ_T^* and c_P upon supercooling. It also describes qualitatively the discontinuous changes in these quantities across water's first-order freezing transition to hexagonal ice.

3.2. Hydrogen bonding structures

In this section, we explore how these properties arise from the microscopic structures of water triplets in this model. Fig. 4 shows the behavior of the local cell populations f_j, $(j=1)$ cage-like, $(j=2)$ dense, and $(j=3)$ expanded vs. temperature for the liquid range at atmospheric pressure, from the coldest supercooled state $(T_r=0)$ to the hottest superheated state (the liquid–vapor spinodal temperature, $T_r \approx 0.8025$). Unbroken vertical lines mark the locations of the first-order freezing and boiling transitions. 'Stable' indicates the temperature range where the liquid has a lower chemical potential than either the vapor or the crystalline phases. 'Supercooled' and 'superheated' denote the temperature ranges where the liquid is metastable with respect to LP ice and the vapor, respectively.

The model explains how heating leads first to increased density, then to decreased density. The coldest supercooled liquid consists of almost entirely hydrogen-bonded cage-like structures. As the supercooled liquid is heated towards the freezing transition, hydrogen bonds are broken, and the liquid cages 'melt' to become dense liquid structures. The stable liquid consists of a combination of cage-like, dense, and expanded triplet configurations. With further increases in temperature, the liquid's volume increases as the cages and dense structures break apart to form expanded structures.

The predicted populations shown in Fig. 4 are compared to water's hydrogen-bond populations as deduced from IR spectroscopic data [31]. Based on an analysis of OH stretching bands, Luck [31]

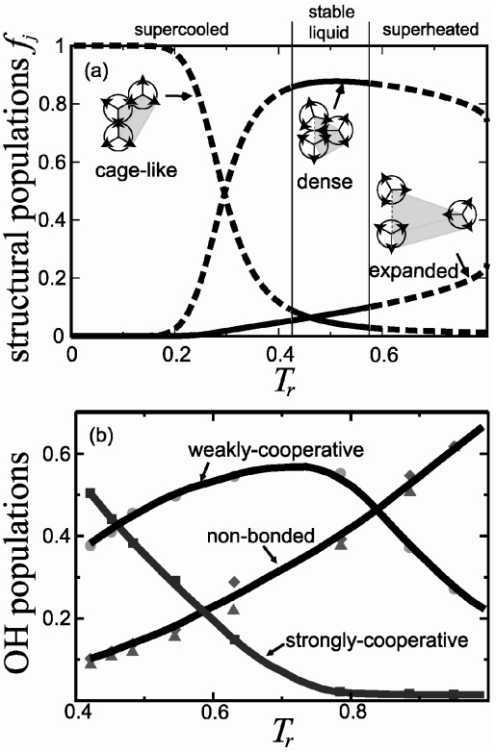

Fig. 4. The temperature dependence of liquid water's structure. (a) Model predictions of structural populations f_j vs temperature T_r at atmospheric pressure (see footnote 1). The vertical lines show the locations of the freezing and boiling points (see Fig. 6). 'Supercooled' indicates liquid that is metastable with respect to freezing. 'Superheated' indicates a liquid that is metastable with respect to boiling. (b) Populations of OH states in liquid water vs. temperature T_r along its saturation curve as determined from IR spectroscopic data (adapted from Fig. 5 of Luck [31]). Curves are guides to the eye.

[1] We choose the model's 'atmospheric' pressure to be $P_r^{\mathrm{atm}}=0.1627$, where it exhibits a reduced freezing temperature of $T_r \approx 0.4255$ and a reduced boiling temperature of $T_r \approx 0.5804$. Inputting water's critical parameters yields a freezing temperature of 2.2 °C and a boiling temperature of 102.4 °C. Thus, at 'atmospheric' pressure P_r^{atm}, the model liquid displays approximately the same range of thermodynamic stability as does liquid water at 1 atm.

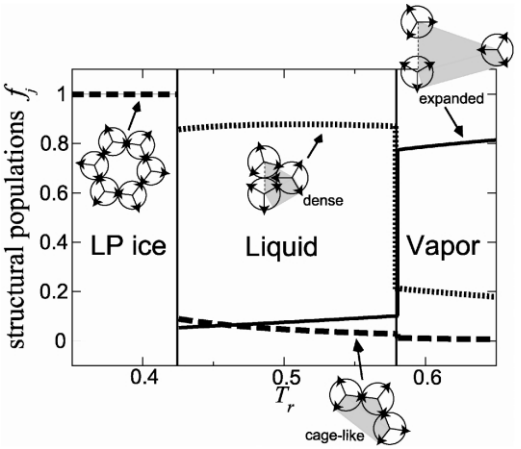

Fig. 5. Structure of the model's crystalline, liquid, and vapor phases at atmospheric pressure (see footnote 1). LP ice has a uniform structure. The liquid and vapor phases are composed populations f_j of $(j=1)$ cage-like, $(j=2)$ dense, and $(j=3)$ expanded triplet structures. The vertical lines indicate the locations of the freezing and boiling points (see Fig. 6).

has identified three distinct types of OH states in the liquid (listed in order of increasing energy): strongly-cooperative hydrogen-bonded, weakly-cooperative hydrogen-bonded, and non-bonded. These states are analogous to our model's cage-like, dense, and expanded energy levels, respectively. Strongly-cooperative hydrogen bonds are prevalent in cold water. Heating melts the strongly-cooperative structures into weakly-cooperative and non-bonded states at intermediate temperatures. The weakly-cooperative hydrogen bonds break to form non-bonded states as the liquid approaches the critical point. The comparison in Fig. 4 shows that the present model captures these experimental observations.

Fig. 5 shows the structural populations of the model's equilibrium phases at atmospheric pressure. At low temperature, LP ice is the stable equilibrium phase, and each molecule participates in exactly three hydrogen bonds. At higher temperatures, LP ice melts into the liquid, which has cage-like, dense, and expanded triplet structures. At even higher temperatures, the liquid boils to become a vapor phase, which is dominated by triplets of water molecules in the expanded state.

3.3. The phase diagram

Fig. 6 compares the phase behavior of the model to the experimental phase diagram for water. The curves locate the phase boundaries in the pressure-temperature plane. These boundaries are calculated [1,2] by determining, for each temperature T, the pressure P at which the chemical potentials of two competing phases are equal.

The model reproduces many of the features of water's phase diagram. For instance, the melting transition for LP ice is negatively-sloped, indicating that the liquid is denser than LP ice along the coexistence curve. At high pressure, LP ice undergoes a first-order transition to HP ice, which exhibits a positively-sloped melting transition. These transitions are qualitatively similar to those involving the experimental low-pressure and high-pressure forms of ice (e.g. Ice I_h and Ice VII, respectively) [32]. The melting and boiling curves converge to a liquid–solid–vapor triple point. In agreement with the phase diagram of water, the

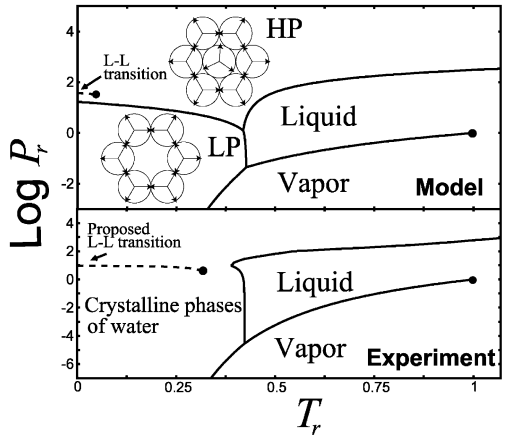

Fig. 6. Phase diagram of water: model (top) and experiments (bottom) in pressure P_r vs temperature T_r. The unbroken curves are the phase boundaries of the phase transitions discussed in the text. For clarity, the many solid–solid transitions in the experimental phase diagram of water have been omitted. The dashed curves are the metastable liquid–liquid transitions discussed in the text. See Mishima and Stanley [8] for a discussion of the proposed liquid–liquid phase transition in supercooled water. The values of the parameters used for the theory are given in Table 2.

triple point temperature is roughly 42% of the vapor–liquid critical temperature.

The model also explains the apparent liquid–liquid transition in supercooled water. It predicts a low-temperature first-order phase transition between two structurally-distinct deeply supercooled liquid phases (shown in Fig. 6)—a high-density liquid (with mostly dense triplet structures) and a low-density liquid (with mostly open, cage-like structures). This is consistent with the view that the 'first-order' transformation [33,34,8] between water's low-density and high-density solid amorphous forms (LDA and HDA, respectively) is an arrested signature of an underlying liquid–liquid transition [7,8]. Experimental verification of this hypothesis has been prevented, so far, by vitrification (glass formation) and crystallization (ice formation) of deeply supercooled water [5,8].

3.4. 'Fragile-to-strong' behavior in water

If crystallization can be avoided when liquid water is cooled, it will form a glass [5]. As the temperature is lowered towards the glass transition, liquid water's structural relaxation time τ increases rapidly, approaching hundreds of seconds. Accordingly, its viscosity $\eta \propto \tau$ increases and its diffusivity $D \propto \tau^{-1}$ decreases.

Angell [35,36] has provided a useful classification for the temperature-dependent relaxation behavior of glass-forming materials. Liquids that show Arrhenius temperature dependencies are called 'strong'; those that exhibit marked deviations from Arrhenius behavior are called 'fragile'. Strong substances, such as the network formers SiO_2 and GeO_2, are able to resist thermal degradation; i.e. their short- and intermediate-range structural order persists to high temperature. On the other hand, key structural features of fragile glass-formers, such as *o*-terphenyl, disappear rapidly upon heating above their glass transition temperature. Water may be a notable exception to this classification [37]. Specifically, supercooled water behaves like a fragile liquid near its freezing temperature, whereas recent evidence indicates that it behaves like a strong liquid near its glass transition temperature [37].

To predict water's kinetics from our model, we use the Adam–Gibbs theory [38], which relates the diffusivity D to the liquid's configurational entropy s_C:

$$D = D_0 \exp\left(-\frac{C}{T s_c}\right) \tag{15}$$

Here, D_0 and C are constants and s_c is usually taken to be the difference between the entropy of the supercooled liquid and the stable crystal at the same temperature and pressure. Our model gives the entropy of all phases and hence, the configurational entropy s_c. Using Eq. (15), we can compute the diffusivity D of the supercooled liquid. Fig. 7 compares the predictions of our theory at atmospheric pressure (see footnote 1) to the experimental data [39]. It shows the predicted fragile-to-strong transition in supercooled water and the corresponding structural transformations in the liquid.

To the extent that water's dynamics are determined by its configurational entropy, as is supposed in the Adam–Gibbs treatment, the present model gives the following explanation for the fragile-to-strong transition. In the coldest supercooled liquid, the dynamics are due to small torsional fluctuations of hydrogen-bonded cage-like structures. The onset of the non-Arrhenius, or fragile, behavior occurs over the reduced temperature range between liquid water's glass transition and homogeneous nucleation temperatures $T_g < T_r < T_h$, where pronounced structural transformations take place in the liquid. The fragility of the model liquid over this range is due to the large increase in configurational entropy that occurs when the orientationally-constrained cage-like structures are melted out, giving way to the orientationally-free dense and expanded states. The mobility of water increases sharply with temperature in this range. Once the cages have melted out, further increases in temperature lead only to small increments in mobility, again following near-Arrhenius behavior.

4. Conclusions

We have reviewed the predictions of a simple model of water in its liquid and solid phases. The

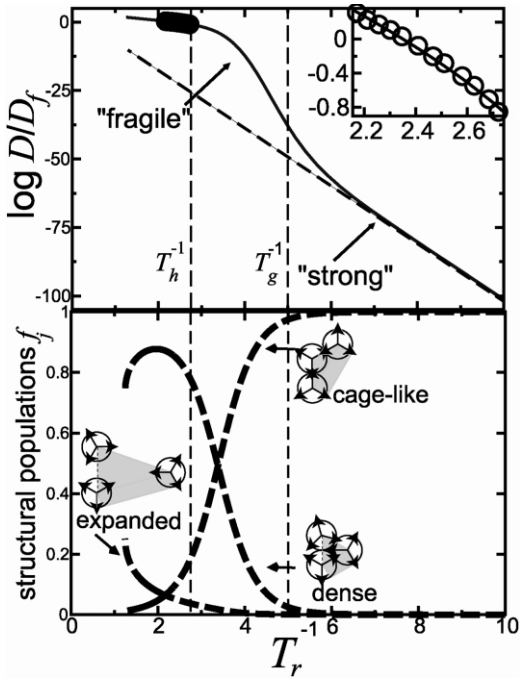

Fig. 7. Log D/D_f vs. reciprocal temperature T_r^{-1}, where D is the self-diffusion coefficient of the liquid and D_f is its value at the freezing transition. The unbroken curve shows model predictions using the Adam–Gibbs theory. D/D_f in Adams–Gibbs theory depends on one free parameter C, which we set to $C=12$ to fit the experimental data [39] (circles) at atmospheric pressure (see footnote 1). The broken slanted line is provided to highlight the crossover from Arrhenius to non-Arrhenius kinetics in the supercooled liquid, i.e. a fragile-to-strong transition. The vertical dashed lines labeled T_g^{-1} and T_h^{-1} show the location of the experimental [8] glass transition and homogeneous nucleation reciprocal temperatures for liquid water.

model treats van der Waals attractions, steric repulsions, and orientation-dependent hydrogen bonding between triplets of neighboring water molecules. It divides water's local structural environments into three classes: cage-like, dense, and expanded structures. This local division captures the connections between energy, volume, and entropy that we believe to be important for water. The model is analytical and offers simple insights into water's behavior, including the density maximum, anomalously large heat capacity, minima in both isothermal compressibility and heat capacity upon isobaric cooling, expansion upon freezing at low pressure, and the conjectured first-order transition between low-temperature amorphous forms. It also predicts qualitatively the proposed fragile-to-strong transition in the temperature dependence of supercooled water's relaxation processes (e.g. its diffusivity). The success of the model suggests that the unusual properties of water arise from the balance between simple centro-symmetric intermolecular attractions and repulsions, on the one hand, and the orientation-dependent hydrogen bonds that impose geometric constraints on the molecular arrangements, on the other.

Acknowledgments

We thank the National Institutes of Health for support.

References

[1] T.M. Truskett, K.A. Dill, Predicting water's phase diagram and liquid-state anomalies, J. Chem. Phys. 117 (2002) 5101–5104.
[2] T.M. Truskett, K.A. Dill, A simple statistical mechanical model of water, J. Phys. Chem. B 106 (2002) 11829–11842.
[3] D. Eisenberg, W. Kauzmann, The structure and properties of water, Oxford University Press, London, 1969.
[4] F.H. Stillinger, Water revisited, Science 209 (1980) 451–457.
[5] P.G. Debenedetti, Metastable Liquids, Princeton University Press, Princeton, 1996.
[6] P. Ball, Life's Matrix: A Biography of Water, Farrar, Straus, and Giroux, New York, 1999.
[7] P.H. Poole, F. Sciortino, U. Essman, H.E. Stanley, Phase behavior of metastable water, Nature 360 (1992) 324–328.
[8] O. Mishima, H.E. Stanley, The relationship between liquid, supercooled and glassy water, Nature 396 (1998) 329–335.
[9] W. Kauzmann, Some factors in the interpretation of protein denaturation, Adv. Protein Chem. 14 (1959) 1–63.
[10] C. Tanford, The Hydrophobic Effect—Formation of Micelles and Biological Membranes, Wiley, New York, 1973.
[11] K.A. Dill, Dominant forces in protein folding, Biochemistry 29 (1990) 7133–7155.
[12] L.R. Pratt, A. Pohorille, Hydrophobic effects and modeling of biophysical aqueous solution interfaces, Chem. Rev. 102 (2002) 2671–2692.
[13] L.R. Pratt, D. Chandler, Theory of the hydrophobic effect, J. Chem. Phys. 67 (1977) 3683–3704.

[14] S. Garde, G. Hummer, A.E. Garcia, M.E. Paulaitis, L.R. Pratt, Origin of entropy convergence in hydrophobic hydration and protein folding, Phys. Rev. Lett. 77 (1996) 4966–4968.
[15] K. Lum, D. Chandler, J.D. Weeks, Hydrophobicity at small and large length scales, J. Phys. Chem. B 103 (1999) 4570–4577.
[16] P.H. Poole, F. Sciortino, T. Grande, H.E. Stanley, C.A. Angell, Effect of hydrogen bonds on the thermodynamic behavior of liquid water, Phys. Rev. Lett. 73 (1994) 1632–1635.
[17] T.M. Truskett, P.G. Debenedetti, S. Sastry, S. Torquato, A single-bond approach to orientation-dependent interactions and its implications for liquid water, J. Chem. Phys. 111 (1999) 2647–2656.
[18] T.M. Truskett, P.G. Debenedetti, S. Torquato, Thermodynamic implications of confinement for a waterlike fluid, J. Chem. Phys. 114 (2001) 2401–2418.
[19] H.S. Ashbaugh, T.M. Truskett, P.G. Debenedetti, A simple molecular thermodynamic theory for hydrophobic hydration, J. Chem. Phys. 116 (2002) 2907–2921.
[20] A. Ben-Naim, Statistical mechanics of 'waterlike' particles in two dimensions. I. Physical model and application of the Percus–Yevick equation, J. Chem. Phys. 54 (1971) 3682–3695.
[21] K.A.T. Silverstein, A.D.J. Haymet, K.A. Dill, A simple model of water and the hydrophobic effect, J. Am. Chem. Soc. 120 (1998) 3166–3175.
[22] K.A.T. Silverstein, A.D.J. Haymet, K.A. Dill, Molecular model of hydrophobic solvation, J. Chem. Phys. 111 (1999) 8000–8009.
[23] N.T. Southall, K.A. Dill, A.D.J. Haymet, A view of the hydrophobic effect, J. Phys. Chem. B 106 (2002) 521–533.
[24] D. Paschek, A. Geiger, Simulation study on the diffusive motion in deeply supercooled water, J. Phys. Chem. B 103 (1999) 4139–4146.
[25] J.R. Errington, P.G. Debenedetti, Relationship between structural order and the anomalies of liquid water, Nature 409 (2001) 318–321.
[26] M.-C. Bellissent-Funel, Is there a liquid–liquid phase transition in supercooled water?, Europhys. Lett. 42 (1998) 161–166.
[27] G.S. Kell, Precise representation of volume properties of water at one atmosphere, J. Chem. Eng. Data 12 (1967) 66–69.
[28] R.J. Speedy, C.A. Angell, Isothermal compressibility of supercooled water and evidence for a thermodynamic singularity at ~45°C, J. Chem. Phys. 65 (1976) 851–858.
[29] C.A. Angell, M. Oguni, W.J. Sichina, Heat capacities of water at extremes of supercooling and superheating, J. Phys. Chem. 86 (1982) 998–1002.
[30] D.E. Hare, C.M. Sorensen, Densities of supercooled H_2O and D_2O in 25 μ glass capillaries, J. Chem. Phys. 84 (1986) 5085–5089.
[31] W.A.P. Luck, The importance of cooperativity for the properties of water, J. Mol. Struct. 448 (1998) 131–142.
[32] V.F. Petrenko, R.W. Whitworth, Physics of Ice, Oxford University Press, New York, 1999.
[33] O. Mishima, L.D. Calvert, E. Whalley, An apparently first-order transition between two amorphous phases of ice induced by pressure, Nature 314 (1985) 76–78.
[34] O. Mishima, Reversible first-order transition between two H2O amorphs at ~0.2 GPa and ~135 K, J. Chem. Phys. 100 (1994) 5910–5912.
[35] C.A. Angell, Relaxation in liquids, polymers, and plastic crystals—strong/fragile patterns and problems, J. Non-Cryst. Solids 131–33 (1991) 13–31.
[36] C.A. Angell, Formation of glasses from liquids and biopolymers, Science 267 (1995) 1924–1935.
[37] K. Ito, C.T. Moynihan, C.A. Angell, Thermodynamic determination of fragility in liquids and fragile-to-strong liquid transition in water, Nature 398 (1999) 492–495.
[38] G. Adam, J.H. Gibbs, On the temperature-dependence of cooperative relaxation properties in glass-forming liquids, J. Chem. Phys. 43 (1965) 139–146.
[39] W.S. Price, H. Ide, Y. Arata, Self-diffusion of supercooled water to 238 K using PGSE NMR diffusion measurements, J. Phys. Chem. A 103 (1999) 448–450.